CARBON letters

Original Articles
Carbon Letters Vol. 23, 9-16 (2017)

Fabrication of nitrogen doped ordered mesoporous carbon derived from glucosamine with hybrid capacitive behaviors

Deyi Zhang[1,2,♠], Mei Han[1], Yubing Li[1], Bing Wang[1], Yi Wang[1], Kunjie Wang[1] and Huixia Feng[1]

[1]College of Petrochemical Technology, Lanzhou University of Technology, Lanzhou 730050, China
[2]Key Laboratory of Eco-Environment-Related Polymer Materials of Ministry of Education, Northwest Normal University, Lanzhou 730070, China

Article Info

Received 1 September 2016
Accepted 23 March 2017

♠Corresponding Author
E-mail: lzdeyizhang@163.com
Tel: +008613919114108

Open Access

DOI: http://dx.doi.org/10.5714/CL.2017.23.009

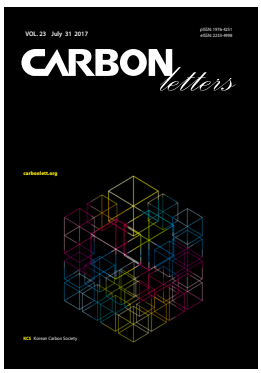

http://carbonlett.org

pISSN: 1976-4251
eISSN: 2233-4998

Abstract

This paper introduces a nitrogen-doped ordered mesoporous carbon (NOMC) derived from glucosamine with hybrid capacitive behaviors, achieved by successfully combining electrical double-layer capacitance with pseudo-capacitance behaviors. The nitrogen doping content of the fabricated NOMC reached 7.4 at% while its specific surface area (S_{BET}) and total pore volume reached 778 $m^2 g^{-1}$ and 1.17 $cm^3 g^{-1}$, respectively. A dual mesoporous structure with small mesopores centered at 3.6 nm and large mesopores centered at 9.9 nm was observed. The specific capacitance of the reported materials reached up to 328 F g^{-1}, which was 2.1 times higher than that of pristine CMK-3. The capacitance retention rate was found to be higher than 87.9% after 1000 charge/discharge cycles. The supplementary pseudo-capacitance as well as the enhanced wettability and conductivity due to the incorporation of nitrogen heteroatoms within the carbon matrixes were found to be responsible for the excellent capacitive performance of the reported NOMC materials.

Key words: nitrogen heteroatoms doping, ordered mesoporous carbon, glucosamine, capacitive performance

1. Introduction

In recent years, faradaic pseudo-capacitance, generated on the surface of nitrogen-doped carbon materials, has been revealed, and its potential application in high performance supercapacitors has attracted extensive interest from researchers [1-4]. In addition to the faradaic pseudo-capacitance, nitrogen doping has also been extensively reported to enhance the electrical conductivity and surface wettability of carbon materials [5,6], and these properties are also beneficial to enhancing capacitive performance. Recently, Lin et al. [1] reported a nitrogen-doped few-layer mesoporous carbon with an extra high specific capacitance of 855 F g^{-1} due to the contribution of faradaic pseudo-capacitance generated by nitrogen-associated defects. In our previous work, we also reported several nitrogen and sulfur co-doped ordered mesoporous carbon materials with pronounced faradaic pseudo-capacitance [2,7].

Because of their well-ordered pore structure, high surface areas, large pore volumes, and excellent surface chemical activity, nitrogen-doped ordered mesoporous carbon (NOMC) materials have been considered ideal electrode materials for high-performance supercapacitors [1,4,8]. Various strategies, such as post-treatment [9,10] and template strategies [11-14], have been developed for synthesizing these novel materials. The main drawback of the post-treatment strategy is that it offers less control over the amount and distribution of dopants. In contrast, the template strategy allows for homogeneous incorporation of nitrogen atoms into the carbon matrix in a controlled fashion [15,16].

When the template approach is used for fabricating NOMCs, the template strategy can be classified into two types, the soft and the hard template approach. The soft template

approach utilizes the organic-organic assembly of the nitrogen-containing precursor and amphiphilic surfactants to construct a nitrogen-rich polymer with ordered mesoporous structure, and then obtains NOMCs through a further carbonization process [17-19]. The soft template approach is a simple and economical method for fabricating NOMCs. The main drawbacks of this approach are the low doping content and inferior textural properties, which are unfavorable for the capacitive performance of NOMCs. In contrast to the soft template approach, the hard template approach fabricates the NOMCs by carbonizing a nitrogen-rich precursor in the ordered mesoporous channels of a silica molecular sieve [4,14]. This allows control over the pore structure, morphology and doping content of the resulting materials. As a result, the hard template approach is the most popular method for obtaining NOMC materials.

The selection of precursors is extremely important for obtaining NOMC materials via the hard template approach. Previously, various nitrogen-enriched organics, such as pyrrole [20,21], cyanamide [4,22], and dicyandiamide [19,23], have been employed as precursors. Unfortunately, these organic precursors exhibit poor thermo-stability, due to the serious decomposition of C–N bonds at the high carbonization temperature, which causes a sharp decrease in the final nitrogen doping content, and destroys the architecture of the NOMC materials. Consequently, this makes it difficult for researchers to produce NOMC materials with high doping content and excellent textural properties.

Glucosamine is a derivative of glucose which is naturally occurring in nature. Besides having a high nitrogen content, each glucosamine molecule possesses four hydroxyl groups, so the carbon framework can be easily formed by intramolecular dehydration when catalyzed by concentrated sulfuric acid.

In this paper, glucosamine was first utilized as a precursor to fabricate NOMC electrode materials via the hard template approach. The fabricated NOMC materials exhibited superior capacitive performance due to the successful combination of the electrical double-layer capacitance (EDLC) and the pseudo-capacitance induced by the nitrogen heteroatoms doping.

2. Experimental

2.1. Synthesis of the SBA-15 template

The SBA-15 template was obtained by following the method reported by Zhao et al. [24]. Briefly, 2.0 g of Pluronic P123 (EO20PO70EO20, MW=5800; Aldrich, USA) was added to a mixed solution of 72 g of distilled water and 4 g of 35% HCl. After complete dissolution, the above mixed solution was vigorously stirred at 35°C for 2 h, and then 4.3 g of tetraethyl orthosilicate (99.9%, Aldrich) was added to the homogeneous clear solution. The mixture was left under stirring for 24 h at 35°C and subsequently heated for 24 h at 100°C in a Teflon-lined autoclave vessel. The solid product obtained was filtered and dried at 100°C, and then the template was removed by extraction in an ethanol−HCl mixture. The SBA-5 template was then obtained after calcination at 550°C under air atmosphere.

2.2. Fabrication of the NOMC material

The NOMC was fabricated by employing a hard template approach using glucosamine as precursor and SBA-15 as template. In brief, 1.0 g of glucosamine was dissolved in a mixed solution of 2.0 mL of deionized water and 0.2 mL of 98 wt% H_2SO_4, and then the solution was slowly dropped onto the surface of 1.0 g of the SBA-15 template. The impregnated template was heated at 110°C for 2 h under vacuum to evaporate redundant solvent and then carbonized under an argon atmosphere at 800°C for 2 h. Finally, the silica template was removed in a HF (10 wt%) aqueous solution to obtain the final materials. For comparison with the textural and capacitance performance of the fabricated materials, a pristine ordered mesoporous carbon CMK-3 with similar morphology and pore structure was synthesized by using sucrose as the precursor.

2.3. Material characterization

Small-angle X-ray scattering (SAXS) measurements were taken on an X'Pert X-ray diffractometer (Phillips, USA). The d spacing values were calculated by the formula $d=\lambda/2\sin\theta$, and the unit cell parameters were calculated from the formula $a=2\times3^{-1/2}d_{100}$. The specific surface areas (S_{BET}) and pore distribution of the samples were measured by a Micromeritics ASAP 2020 volumetric adsorption analyzer (USA) at 77 K. The X-ray photoelectron spectroscopy (XPS; Thermo Multilab 2000 instrument, USA) was employed to determine the elements' composition and their chemical environment. A scanning electron microscope (S-4800; Hitachi, Japan) and transmission electron microscope (TEM; JEM-2010, Jeol, Japan) were employed to observe the morphology and shape of the fabricated NOMC materials.

2.4. Electrochemical measures

All electrochemical experiments were performed on a CHI 660E electrochemical workstation using a three-electrode system in a 2M KOH electrolyte solution, with the fabricated materials as the working electrode, a platinum slice and saturated calomel electrode as the counter and reference electrodes, respectively. The working electrode was prepared by mixing a certain sample of the fabricated materials (ca., 5 mg), acetylene black and polytetrafluoroethylene with a weight ratio of 85:10:5, and then coating the above slurry mixture on foamed Ni grids (10 mm×10 mm), which were subsequently dried at 80°C for 24 h and compressed at a pressure of 10 MPa. The specific capacitance C was calculated from the galvanostatic charge/discharge curves based on the following equation:

$$C = \frac{I\Delta t}{m\Delta V} \quad (1)$$

where I refers to the discharge current (A), m represents the mass of the active material (g), Δt represents the discharge time (s), and ΔV is the discharge potential range (V).

3. Results and Discussion

The surface chemical compositions and atomic content of the fabricated NOMC materials were determined by XPS technique. As shown in Fig. 1a, C was still the dominant surface element, and its content reached 88.7 at% after heteroatom doping.

In addition to the C atoms, pronounced amounts of N and O were also detected, and their content reached 7.4 and 3.9 at%, respectively. To verify the chemical circumstances of the N heteroatoms, high-resolution XPS spectra of the N 1s orbit were deconvoluted, and the results are presented in Fig. 1b. As shown in Fig. 1b, the XPS spectra of the N 1s orbit for the fabricated NOMC materials displays three peaks, centered at 398.5, 400.3, and 401.1 eV, respectively. The peak with a binding energy centered at 398.5 eV was identified as the pyridinic-like N species (N1), which is bound to two adjacent carbon atoms and mainly located at the edges of the graphene layers. The peak centered at 400.3 eV corresponds to the pyrrolic-like N species in a five-membered carbon ring (N2), and the peak around 401.1 eV can be assigned to the graphite-like N species (N3), which was incorporated into the graphene layer by replacing a carbon atom within the graphene plane [1,25-27].

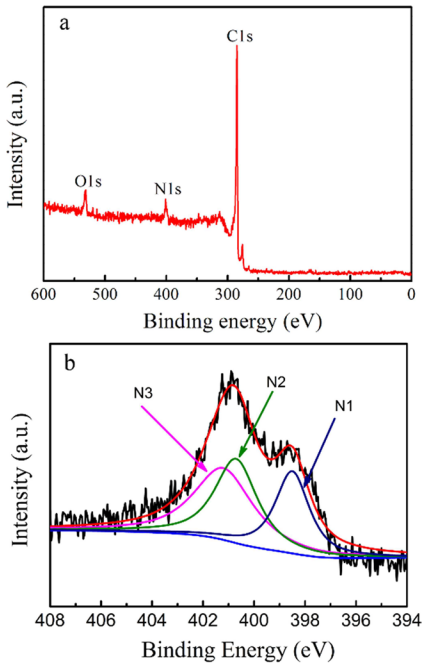

Fig. 1. X-ray photoelectron spectroscopy (XPS) spectra of fabricated nitrogen-doped ordered mesoporous carbon materials (a), and high-resolution XPS spectra of the N 1s orbit (b).

The relative content of the graphite-like N species was found to be more than 40% of the total N doping content while that of the pyridinic-like and pyrrolic-like N species reached 26.5 and 33.5%, respectively. Pyridinic-like and pyrrolic-like N species have previously been reported to be responsible for the additional pseudo-capacitance in nitrogen-doped carbon materials, while the graphite-like N species contribute to the enhanced conductivity and wettability [1,2], so it was reasonable to expect the fabricated NOMC materials to exhibit excellent capacitive performance.

Besides the N heteroatoms, pronounced amounts of O atoms were detected on the material's surface. However, no perceptible peaks were observed of oxidized nitrogen species, such as —NO_x, as shown in Fig. 1b, indicating that the O atoms on the surface were mainly bound to C atoms rather than N atoms. The abundant oxygen-containing functional groups on the surface would be favorable to the fast transfer and diffusion of electrolytic ions in mesoporous tunnels, and thus enhanced the capacitive performance of the fabricated NOMC materials.

In addition to the high heteroatom doping content, the fabricated NOMC materials also exhibited excellent textural properties. As shown in Table 1, the S_{BET} and the mesopore volume values calculated using the rate of the nitrogen adsorption-desorption isotherm reached 778 $m^2\ g^{-1}$ and 1.17 $cm^3\ g^{-1}$, respectively. Although the CMK-3 and NOMC samples were fabricated using a similar strategy, the S_{BET} value for the CMK-3 was found to be higher than that of the NOMC. The sharp decrease in the S_{BET} value of the NOMC may be due to the more advanced pyrolysis of glucosamine during the carbonization process, compared to the sucrose which was used as the precursor for fabricating the CMK-3. The intense pyrolysis induced the collapse of mesoporous channels, which resulted in a sharp decrease in S_{BET} values.

Meanwhile, no apparent micropores or macropores were detected for the NOMC sample. However, a lot of micropores were detected for the CMK-3: mesopore volume only accounted for 89.9% of the total pore volume. The nitrogen adsorption-desorption isotherms of the fabricated NOMC materials, as shown in Fig. 2a, exhibited typical type IV adsorption isotherms with an apparent H1 hysteresis loop at relative pressures from 0.4 to 0.9, indicating the mesoporous nature of the fabricated NOMC materials. The initiative pressure of the hysteresis loops in the pristine CMK-3 and the fabricated NOMC materials was lower than that of the SBA-15 template, implying a lower pore diameter for the pristine CMK-3 and the fabricated NOMC materials than that of the SBA-15 template [28].

Meanwhile, the slope of the hysteresis loop indicates a consistent uniformity in pore diameter. As shown in Fig. 2a,

Table 1. Textural parameters of the fabricated NOMC material

Sample ID	d_{100} (nm)	a (nm)	D_p (nm)	D_{av} (nm)	S_{BET} ($m^2\ g^{-1}$)	V_T ($cm^3\ g^{-1}$)	V_M ($cm^3\ g^{-1}$)
SBA-15	9.50	10.97	9.58	6.73	930	1.44	1.34
CMK-3	8.33	9.62	3.43	3.53	1480	1.59	1.43
NOMC	8.13	9.39	3.61, 9.93	4.59	778	1.17	1.17

NOMC, nitrogen-doped ordered mesoporous carbon; D_p, pore diameter; D_{av}, average pore diameter; S_{BET}, specific surface area.

the hysteresis loop initiative pressure of the fabricated NOMC materials was similar to that of the pristine CMK-3, however, the slope of the hysteresis loop of the fabricated NOMC materials was lower than that of the pristine CMK-3. This indicates that, while the fabricated NOMC materials had a pore structure similar to the pristine CMK-3, the uniformity of the pore diameter was inferior to the pristine CMK-3. The inferior pore uniformity was mainly due to the dual-mesoporous structure of the fabricated NOMC materials.

As shown in Fig. 2b, the pore size distribution curves of the fabricated NOMC materials exhibited 2 sharp peaks at 3.6 and 9.9 nm, respectively. Both the CMK-3 and NOMC were fabricated via a nanocasting strategy which employed SBA-15 as a hard template. Because the samples are successful reversed duplicates of the SBA-15 template, in theory the predominant pore diameter (3.6 nm) of the pristine CMK-3 and NOMC should be very close to the wall thickness of the SBA-15 (4.39 nm). But due to framework shrinkage during the carbonization process of the precursor, the pore diameters of the CMK-3 and NOMC materials were lower than the pore wall thickness of the SBA-15.

Beside the small mesopores, larger mesopores with a pore diameter of 9.9 nm were also observed in the fabricated NOMC materials. Considering that the pore diameters of the larger mesopores within the cell parameters of the SBA-15 were similar (as shown in Table 1), the larger mesopores may have been generated by unfilled mesopores in the SBA-15, due to poor filling by the precursor.

The ordered mesoporous structure of the fabricated NOMC materials was identified by SAXS patterns. As shown in Fig. 3, 3 characteristic diffraction peaks associated with the 100, 110, and 200 reflections of 2D hexagonal symmetry with the space group of *p6mm* were clearly observed [4,29]. The fabricated NOMC materials exhibited a SAXS pattern similar to that of the template SBA-15, confirming that the ordered mesoporous structure of the template SBA-15 was truly replicated.

Meanwhile, the diffraction peaks of the fabricated NOMC materials apparently shifted toward a higher angle, implying apparent framework shrinkage during the carbonization process. As shown in Table 1, the cell parameter (a) of the fabricated NOMC materials was calculated to be 9.39 nm, which was lower than that of the SBA-15 template (10.97 nm).

The ordered mesoporous structure of the fabricated NOMC materials was further confirmed by scanning electron microscope (Fig. 4a and b) and TEM images (Fig. 4c and d). As shown in Fig. 4a and b, the carbon rods are orderly and stacked along the axial direction, and form a pea-like morphology. The TEM images show the well-ordered mesoporous structure, and imag-

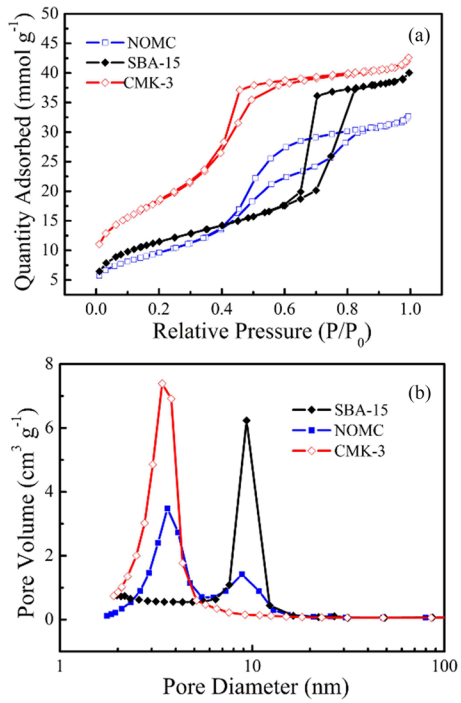

Fig. 2. Nitrogen adsorption-desorption isotherms (a), and pore size distributions (b) of the fabricated nitrogen-doped ordered mesoporous carbon (NOMC) materials.

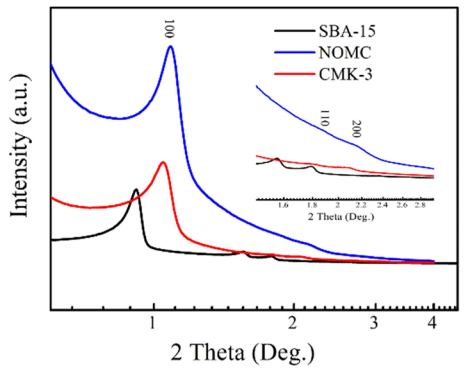

Fig. 3. Small-angle X-ray scattering patterns of the fabricated nitrogen-doped ordered mesoporous carbon (NOMC) materials.

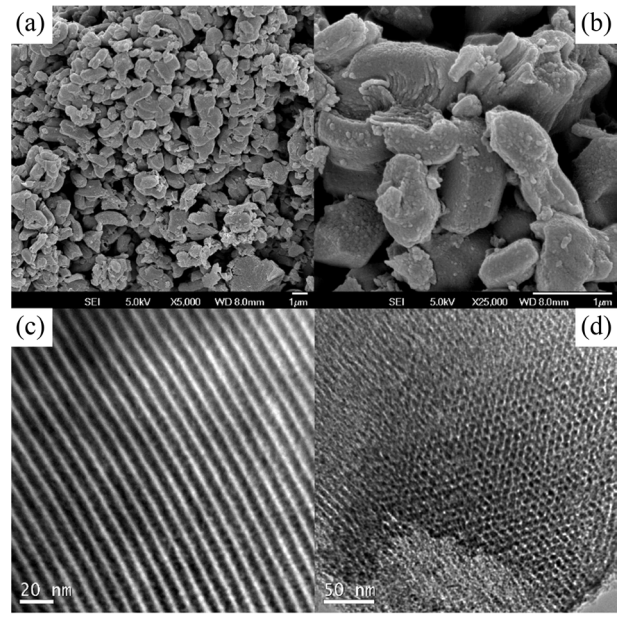

Fig. 4. Typical scanning electron microscope (a, b), and transmission electron microscope (c, d) images of the fabricated nitrogen-doped ordered mesoporous carbon materials.

DOI: http://dx.doi.org/10.5714/CL.2017.23.009

es of the uniform stripe-like (Fig. 4c) and hexagonally arranged (Fig. 4d) structures of the 2D hexagonal symmetry, where the space group of *p6mm* can be clearly observed.

Fig. 5a presents the cyclic voltammetry (CV) curves of the fabricated NOMC and pristine CMK-3 materials obtained at a scan rate of 5 mv s^{-1}. In an ideal electrical double layer capacitor, energy must be retrievable as a discharge over the same potential range as that required to store the energy on charging, which is reflected in the rectangular-shape cyclic voltammograms [30,31]. The pseudo-capacitance associated with the fast and reversible oxidation/reduction (redox) or faradaic charge transfer reactions, are reflected in the reversible redox peaks [32,33] on the CV curves. The rectangular-like CV shape is overlapped by the reversible redox peaks, indicating the concurrence of both EDLC and pseudo-capacitance.

As shown in Fig. 5a, the rectangular-like CV shape of the pristine CMK-3 electrode indicates its EDLC nature. However, the rectangular-like shape is overlapped by at least two pairs of approximately reversible redox peaks in the CV curve of the fabricated NOMC electrode, and this suggests that both the EDLC and the pseudo-capacitance contributed to the charge storage/release capability of the fabricated NOMC electrode. It also indicates that the EDLC and pseudo-capacitance were successfully incorporated and dramatically improved the capacitive performance of the fabricated NOMC electrode.

Even so, the area of the approximate rectangular shape was far more than that of the redox peaks, illustrating that the electrical double layer capacitance still was the primary charge storage/release mechanism, while the pseudo-capacitance made a supplementary contribution.

Meanwhile, as shown in Fig. 5b, although the entire area of the CV curve proportionally increased with the increasing scan rate, the peaks induced by the pseudo-capacitance gradually weakened, indicating that the contribution of the pseudo-capacitance gradually declined with the increasing scan rate. Even so, the peak induced by the pseudo-capacitance was still distinguishable at a high scan rate of 100 mV s^{-1}, indicating the contribution of the pseudo-capacitance was not negligible, even under high scan rate.

Fig. 5c presents the galvanostatic charge/discharge curves of the fabricated NOMC and CMK-3 electrodes at a current density of 0.5 A g^{-1}. As shown in Fig. 5c, the nearly triangular charge/discharge curves for the CMK-3 electrode reveal its ideal electrical double layer capacitive behavior, but for the fabricated NOMC electrode, apparent voltage plateaus can be observed, verifying the contribution of the pseudo-capacitance again.

As a result of the composite capacitive behaviors, the reported materials exhibit a surprising capacity. The specific capacitance calculated from the discharge curves reached 328 F g^{-1} at a current density of 0.5 A g^{-1} for the NOMC electrode, a value which was 2.1 times higher than that of the pristine CMK-3 electrode. Although possessing a high S_{BET} of 1480 m^2 g^{-1}, the specific capacitance of the CMK-3 electrode only reached 157 F g^{-1}.

The dramatic improvement in specific capacitance after nitrogen doping indicates that incorporating nitrogen heteroatoms within the carbon framework can effectively enhance the capacitance performance of ordered mesoporous carbon materials. It was previously reported that pyridinic-like and pyrrolic-like nitrogen at the periphery of the graphene layers resulted in the attraction of ions, such as protons, and consequently induced pseudo-capacitive interactions [7]. Meanwhile, nitrogen heteroatoms doping contributed to improve the wettability of the carbon matrix by modifying its surface polarity [1,2]. Together, the supplementary pseudo-capacitance as well as the enhanced wettability were responsible for the excellent capacitance performance of the fabricated NOMC materials.

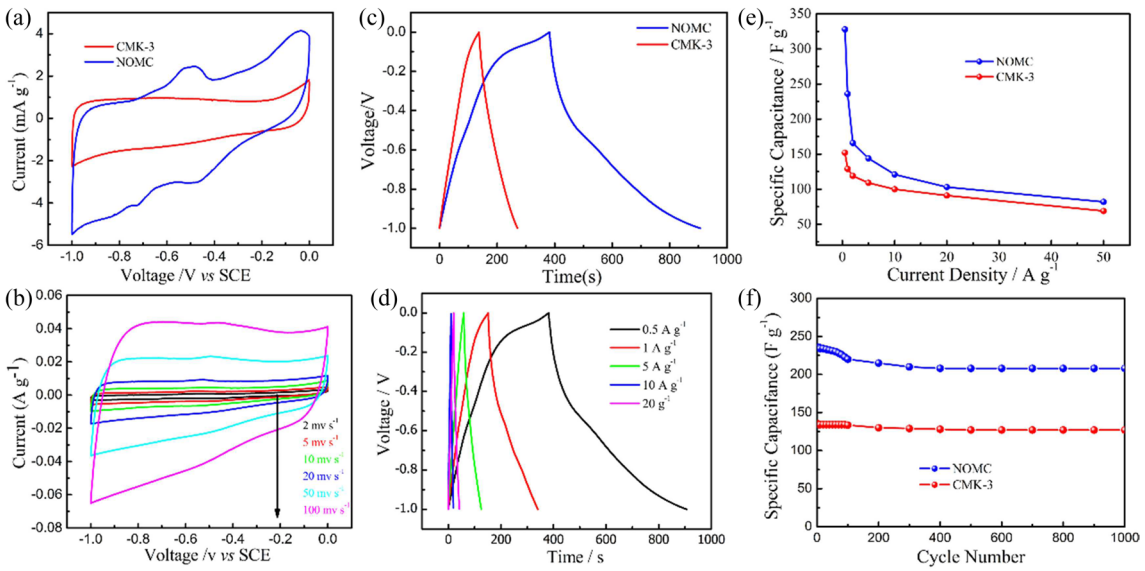

Fig. 5. Cyclic voltammetry (CV) curve of the fabricated NOMC electrode at a scan rate of 5 mV s^{-1} (a), and 2–100 mV s^{-1} (b); galvanostatic charge/discharge curves of the fabricated NOMC electrode under a current density of 0.5 A g^{-1} (c), and different current densities (d); the influence of current densities on the specific capacitances (e); the cycle performance of the fabricated NOMC electrode (f). NOMC, nitrogen-doped ordered mesoporous carbon; SCE, saturated calomel electrode.

However, the decay in the contribution of the pseudo-capacitance with increasing current density was still unavoidable. As shown in Fig. 5d, apparent charge/discharge voltage plateaus can be clearly observed at relatively lower current densities, but these plateaus gradually weaken with the increasing current density. These results suggest that the supplementary pseudo-capacitance only contributed significantly to the capacitance performance of the fabricated NOMC materials under relatively lower current density, and that the electrical double layer capacitance still made a dominant contribution, especially under high current density.

The influence of current densities on the specific capacitances are presented in Fig. 5e. As shown in Fig. 5e, the capacitance of the fabricated NOMC electrode sharply decreased when the current density was increased from 0.5 to 2 A g^{-1}. After that, the decreasing tendency in specific capacitance with increasing current densities is similar to that of the pristine CMK-3. This may be because current density has a significant effect on the pseudo-capacitance, but its effect on the electrical double layer capacitance was unremarkable.

With the increasing current density, the pseudo-capacitance sharply weakened, and resulted in a sharp decrease in specific capacitance under relatively low current density. Even so, the specific capacitance of the fabricated NOMC electrode was still higher than that of the pristine CMK-3, even under a high current density of 50 A g^{-1}, indicating that the fabricated NOMC materials are a more ideal electrode material for a high-performance supercapacitor.

The cycling stability of the NOMC and pristine CMK-3 electrodes was examined using galvanostatic charge/discharge cycling at a current density of 1 A g^{-1} for 1000 cycles, and is presented in Fig. 5f. After 1000 charge/discharge cycles, although the capacitance retention rate of the NOMC electrode was somewhat less than that of the pristine CMK-3, the specific capacitances of the NOMC electrode still reached 208 F g^{-1}, and this value was far higher than that of the pristine CMK-3. The capacitance retention rate of the NOMC electrode reached 87.9% while that of the CMK-3 reached 91.3% after 1000 charge/discharge cycles.

Fig. 6 presents the electrochemical impedance spectroscopy of the fabricated NOMC and pristine CMK-3 materials in 2M KOH solution. As shown in Fig. 6, the Nyquist plots of the NOMC electrode exhibited the typical features of porous electrodes with a 45° Warburg region at high-medium frequencies. Meanwhile, the Nyquist plots exhibited an apparent incline toward the horizontal axis at low frequencies, which may be due to strong interactions between the surface of the fabricated materials and the electrolyte ions, due to the abundant oxygen-containing groups on the surface, and the doped N heteroatoms. At sufficiently high frequencies, the intercept at the real impedance (Z′) axis is related to the internal resistance, including the resistance of the bulk electrolyte, the intrinsic resistance of the electrode materials and their contact resistance with the Ni foam current collector. The internal resistance of the fabricated NOMC materials was found to be 0.92 Ω, a value lower than that of the pristine CMK-3 (1.11 Ω), indicating that the conductivity of the carbon materials can be effectively enhanced by nitrogen heteroatoms doping.

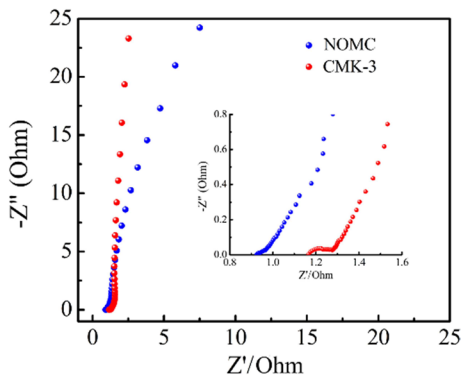

Fig. 6. Nyquist plots of the fabricated nitrogen-doped ordered mesoporous carbon (NOMC) and pristine CMK-3 electrode.

4. Conclusions

NOMC materials with excellent textural properties and high doping content were fabricated by using glucosamine as precursor via the hard template approach. The S_{BET} and the total pore volume of the fabricated NOMC materials reached 778 m^2 g^{-1} and 1.17 cm^3 g^{-1}, and the doping content of the nitrogen heteroatoms was found to be more than 7.4 at%. The fabricated NOMC materials exhibited a dual mesoporous structure: the small mesopores originated from the reverse duplication of the pore structure of the SBA-15 centered at 3.6 nm, while the large mesopores, centered at 9.9 nm, were caused by missing precursor fill.

By successfully combining the effects of EDLC with pseudo-capacitance, the fabricated NOMC materials exhibited hybrid capacitive behaviors. The specific capacitance of the fabricated NOMC materials reached up to 328 F g^{-1} at a current density of 0.5 A g^{-1}, which was 2.1 times higher than that of pristine CMK-3. Meanwhile, good cycle stability was demonstrated, with a high capacitance retention rate after 1000 cycles. The supplementary pseudo-capacitance as well as the enhanced wettability and conductivity are considered responsible for the excellent capacitive performance of the fabricated NOMC materials.

Conflict of Interest

No potential conflict of interest relevant to this article was reported.

Acknowledgements

This work was supported by the National Natural Science Foundation of China (Grant No. 51462020), the Key Laboratory of Eco-Environment-Related Polymer Materials of the Ministry of Education Program (Grant No. KF-13-01) and the Hongliu Young Teacher Cultivate Project of Lanzhou University of Technology (Grant No. Q201112).

References

[1] Lin T, Chen IW, Liu F, Yang C, Bi H, Xu F, Huang F. Nitrogen-doped mesoporous carbon of extraordinary capacitance for electrochemical energy storage. Science, **350**, 1508 (2015). http://doi.org/10.1126/science.aab3798.

[2] Zhang D, Zheng L, Ma Y, Lei L, Li Q, Li Y, Luo H, Feng H, Hao Y. Synthesis of nitrogen- and sulfur-codoped 3D cubic-ordered mesoporous carbon with superior performance in supercapacitors. ACS Appl Mater Interfaces, **6**, 2657 (2014). http://doi.org/10.1021/am405128j.

[3] Zhou J, Zhang Z, Xing W, Yu J, Han G, Si W, Zhuo S. Nitrogen-doped hierarchical porous carbon materials prepared from meta-aminophenol formaldehyde resin for supercapacitor with high rate performance. Electrochim Acta, **153**, 68 (2015). http://doi.org/10.1016/j.electacta.2014.11.075.

[4] Shi Q, Zhang R, Lv Y, Deng Y, Elzatahrya AA, Zhao D. Nitrogen-doped ordered mesoporous carbons based on cyanamide as the dopant for supercapacitor. Carbon, **84**, 335 (2015). http://doi.org/10.1016/j.carbon.2014.12.013.

[5] Einert M, Wessel C, Badaczewski F, Leichtweiß T, Eufinger C, Janek J, Yuan J, Antonietti M, Smarsly BM. Nitrogen-doped carbon electrodes: influence of microstructure and nitrogen configuration on the electrical conductivity of carbonized polyacrylonitrile and poly(ionic liquid) blends. Macromol Chem Phys, **216**, 1930 (2015). http://doi.org/10.1002/macp.201500169.

[6] Hou J, Cao C, Idrees F, Ma X. Hierarchical porous nitrogen-doped carbon nanosheets derived from silk for ultrahigh-capacity battery anodes and supercapacitors. ACS Nano, **9**, 2556 (2015). https://doi.org/10.1021/nn506394r.

[7] Zhang D, Lei L, Shang Y, Wang K, Wang Y. The composite capacitive behaviors of the N and S dual doped ordered mesoporous carbon with ultrahigh doping level. Appl Surf Sci, **360**, 807 (2016). http://doi.org/10.1016/j.apsusc.2015.11.071.

[8] Zhou DD, Li WY, Dong XL, Wang YG, Wang CX, Xia YY. A nitrogen-doped ordered mesoporous carbon nanofiber array for supercapacitors. J Mater Chem A, **1**, 8488 (2013). http://doi.org/10.1039/c3ta11667k.

[9] Wang X, Lee JS, Zhu Q, Liu J, Wang Y, Dai S. Ammonia-treated ordered mesoporous carbons as catalytic materials for oxygen reduction reaction. Chem Mater, **22**, 2178 (2010). http://doi.org/10.1021/cm100139d.

[10] Wang X, Liu CG, Neff D, Fulvio PF, Mayes RT, Zhamu A, Fang Q, Chen G, Meyer HM, Jang BZ, Dai S. Nitrogen-enriched ordered mesoporous carbons through direct pyrolysis in ammonia with enhanced capacitive performance. J Mater Chem A, **1**, 7920 (2013). http://doi.org/10.1039/C3TA11342F.

[11] Sheng X, Daems N, Geboes B, Kurttepeli M, Bals S, Breugelmans T, Hubin A, Vankelecom IFJ, Pescarmona PP. N-doped ordered mesoporous carbons prepared by a two-step nanocasting strategy as highly active and selective electrocatalysts for the reduction of O_2 to H_2O_2. Appl Catal B, **176**, 212 (2015). http://doi.org/10.1016/j.apcatb.2015.03.049.

[12] Lu J, Bo X, Wang H, Guo L. Nitrogen-doped ordered mesoporous carbons synthesized from honey as metal-free catalyst for oxygen reduction reaction. Electrochim Acta, **108**, 10 (2013). http://doi.org/10.1016/j.electacta.2013.06.066.

[13] Zhou S, Xu H, Yuan Q, Shen H, Zhu X, Liu Y, Gan W. N-doped ordered mesoporous carbon originated from a green biological dye for electrochemical sensing and high-pressure CO_2 storage. ACS Appl Mater Interfaces, **8**, 918 (2016). http://doi.org/10.1021/acsami.5b10502.

[14] Yang DS, Bhattacharjya D, Song MY, Razmjooei F, Ko J, Yang QH, Yu JS. Nitrogen-doped ordered mesoporous carbon with different morphologies for the oxygen reduction reaction: effect of iron species and synergy of textural properties. ChemCatChem, **7**, 2882 (2015). http://doi.org/10.1002/cctc.201500340.

[15] Wang G, Zhang J, Kuang S, Zhou J, Xing W, Zhuo S. Nitrogen-doped hierarchical porous carbon as an efficient electrode material for supercapacitors. Electrochim Acta, **153**, 273 (2015). http://doi.org/10.1016/j.electacta.2014.12.006.

[16] Song LT, Wu ZY, Liang HW, Zhou F, Yu ZY, Xu L, Pan Z, Yu SH. Macroscopic-scale synthesis of nitrogen-doped carbon nanofiber aerogels by template-directed hydrothermal carbonization of nitrogen-containing carbohydrates. Nano Energy, **19**, 117 (2016). http://doi.org/10.1016/j.nanoen.2015.10.004.

[17] Shen G, Sun X, Zhang H, Liu Y, Zhang J, Meka A, Zhou L, Yu C. Nitrogen-doped ordered mesoporous carbon single crystals: aqueous organic-organic self-assembly and superior supercapacitor performance. J Mater Chem A, **3**, 24041 (2015). https://doi.org/10.1039/c5ta06129f.

[18] Wei J, Zhou D, Sun Z, Deng Y, Xia Y, Zhao D. A controllable synthesis of rich nitrogen-doped ordered mesoporous carbon for CO_2 capture and supercapacitors. Adv Funct Mater, **23**, 2322 (2013). http://doi.org/10.1002/adfm.201202764.

[19] Song Y, Li L, Wang Y, Wang C, Guo Z, Xia Y. Nitrogen-doped ordered mesoporous carbon with a high surface area, synthesized through organic–inorganic coassembly, and its application in supercapacitors. ChemPhysChem, **15**, 2084 (2014). http://doi.org/10.1002/cphc.201402250.

[20] Wan K, Long GF, Liu MY, Du L, Liang ZX, Tsiakaras P. Nitrogen-doped ordered mesoporous carbon: synthesis and active sites for electrocatalysis of oxygen reduction reaction. Appl Catal B, **165**, 566 (2015). http://doi.org/10.1016/j.apcatb.2014.10.054.

[21] Long G, Wan K, Liu M, Li X, Liang Z, Piao J. Effect of pyrolysis conditions on nitrogen-doped ordered mesoporous carbon electrocatalysts. Chin J Catal, **36**, 1197 (2015). http://doi.org/10.1016/s1872-2067(15)60912-3.

[22] Chen H, Zhou M, Wang Z, Zhao S, Guan S. Rich nitrogen-doped ordered mesoporous phenolic resin-based carbon for supercapacitors. Electrochim Acta, **148**, 187 (2014). http://doi.org/10.1016/j.electacta.2014.10.042.

[23] Li J, Li Z, Tong J, Xia C, Li F. Nitrogen-doped ordered mesoporous carbon sphere with short channel as an efficient metal-free catalyst for oxygen reduction reaction. RSC Adv, **5**, 70010 (2015). http://doi.org/10.1039/C5RA10484J.

[24] Zhao D, Feng J, Huo Q, Melosh N, Fredrickson GH, Chmelka BF, Stucky GD. Triblock copolymer syntheses of mesoporous silica with periodic 50 to 300 angstrom pores. Science, **279**, 548 (1998). http://doi.org/10.1126/science.279.5350.548.

[25] Qiu B, Pan C, Qian W, Peng Y, Qiu L, Yan F. Nitrogen-doped mesoporous carbons originated from ionic liquids as electrode materials for supercapacitors. J Mater Chem A, **1**, 6373 (2013). http://doi.org/10.1039/C3TA10774D.

[26] Chen P, Wang LK, Wang G, Gao MR, Ge J, Yuan WJ, Shen YH, Xie AJ, Yu SH. Nitrogen-doped nanoporous carbon nanosheets derived from plant biomass: an efficient catalyst for oxygen reduction reac-

tion. Energy Environ Sci, **7**, 4095 (2014). http://doi.org/10.1039/C4EE02531H.

[27] Liu H, Jia M, Cao B, Chen R, Lv X, Tang R, Wu F, Xu B. Nitrogen-doped carbon/graphene hybrid anode material for sodium-ion batteries with excellent rate capability. J Power Sources, **319**, 195 (2016). http://doi.org/10.1016/j.jpowsour.2016.04.040.

[28] Lei Z, Xiao Y, Dang L, Lu M, You W. Fabrication of ultra-large mesoporous carbon with tunable pore size by monodisperse silica particles derived from seed growth process. Microporous Mesoporous Mater, **96**, 127 (2006). http://doi.org/10.1016/j.micromeso.2006.06.031.

[29] Zhang M, Sun A, Meng Y, Wang L, Jiang H, Li G. High activity ordered mesoporous carbon-based solid acid catalyst for the esterification of free fatty acids. Microporous Mesoporous Mater, **204**, 210 (2015). http://doi.org/10.1016/j.micromeso.2014.11.027.

[30] Vix-Guterl C, Saadallah S, Jurewicz K, Frackowiak E, Reda M, Parmentier J, Patarin J, Beguin F. Supercapacitor electrodes from new ordered porous carbon materials obtained by a templating procedure. Mater Sci Eng B, **108**, 148 (2004). http://doi.org/10.1016/j.mseb.2003.10.096.

[31] Li ZY, Akhtar MS, Yang OB. Supercapacitors with ultrahigh energy density based on mesoporous carbon nanofibers: enhanced double-layer electrochemical properties. J Alloys Compd, **653**, 212 (2015). http://doi.org/10.1016/j.jallcom.2015.08.275.

[32] Zhang K, Zhang LL, Zhao XS, Wu J. Graphene/polyaniline nanofiber composites as supercapacitor electrodes. Chem Mater, **22**, 1392 (2010). http://doi.org/10.1021/cm902876u.

[33] Laheäär A, Przygocki P, Abbas Q, Béguin F. Appropriate methods for evaluating the efficiency and capacitive behavior of different types of supercapacitors. Electrochem Commun, **60**, 21 (2015). http://doi.org/10.1016/j.elecom.2015.07.022.